Inorg. Chem. **2005**, *44*, 7078–7086

Polymorphic One-Dimensional $(N_2H_4)_2ZnTe$: Soluble Precursors for the Formation of Hexagonal or Cubic Zinc Telluride

David B. Mitzi*

T. J. Watson Research Center, IBM, Post Office Box 218, Yorktown Heights, New York 10598

Received May 23, 2005

Two hydrazine zinc(II) telluride polymorphs, $(N_2H_4)_2ZnTe$, have been isolated, using ambient-temperature solution-based techniques, and the crystal structures determined: α-$(N_2H_4)_2ZnTe$ (**1**) [*P*21, $a = 7.2157(4)$ Å, $b = 11.5439(6)$ Å, $c = 7.3909(4)$ Å, $\beta = 101.296(1)°$, $Z = 4$] and β-$(N_2H_4)_2ZnTe$ (**2**) [*Pn*, $a = 8.1301(5)$ Å, $b = 6.9580(5)$ Å, $c = 10.7380(7)$ Å, $\beta = 91.703(1)°$, $Z = 4$]. The zinc atoms in **1** and **2** are tetrahedrally bonded to two terminal hydrazine molecules and two bridging tellurium atoms, leading to the formation of extended one-dimensional (1-D) zinc telluride chains, with different chain conformations and packings distinguishing the two polymorphs. Thermal decomposition of $(N_2H_4)_2ZnTe$ first yields crystalline wurtzite (hexagonal) ZnTe at temperatures as low as 200 °C, followed by the more stable zinc blende (cubic) form at temperatures above 350 °C. The 1-D polymorphs are soluble in hydrazine and can be used as convenient precursors for the low-temperature solution processing of p-type ZnTe semiconducting films.

Introduction

Recently, we reported the synthesis of soluble hydrazinium-based metal chalcogenide salts that can be used as precursors for the solution deposition of high-mobility semiconducting films.[1] Selected main-group-metal sulfides and selenides dissolve in hydrazine/chalcogen mixtures at room temperature.[1−4] Evaporation of the hydrazine solvent leads to the formation of the salt precursors, in which hydrazinium cations counterbalance isolated anionic metal chalcogenide moieties [e.g., $(N_2H_5)_4Sn_2S_6$, $(N_2H_4)_3(N_2H_5)_4Sn_2Se_6$, $(N_2H_5)_4Ge_2Se_6$]. These precursors cleanly decompose at relatively low temperature, yielding the corresponding metal chalcogenide semiconductor. By spin-coating the precursor directly from the hydrazine-based solution, metal chalcogenide film deposition has been demonstrated for the tin(IV) chalcogenides, with continuous thin films achieved for thicknesses as low as 40 Å. Additionally, n-type indium(III) selenide films have been spin-coated, using the corresponding hydrazinium precursor and mixed ethanolamine/DMSO solvents.[4] Thin-film field-effect transistors (TFTs) have been constructed, based on the solution-deposited semiconducting chalcogenides, yielding n-type channels with electron mobilities in excess of 10 $cm^2\ V^{-1}\ s^{-1}$—approximately an order of magnitude better than previous results for spin-coated semiconductors.[1,2,4] The low-temperature solution-based nature of the hydrazinium precursor approach renders the process attractive for potential use in a number of low-cost and/or large-area applications, including those requiring flexible plastic substrates.

In each of the above examples, the metal chalcogenide under consideration involves a group III or group IV metal and either sulfur or selenium as the chalcogen. To further explore this solution-based route to metal chalcogenide materials and films, it is interesting to consider whether the process can be extended beyond the family of main-group-metal systems and whether tellurides will exhibit similar chemistry. In addition, all of the films previously deposited using the hydrazinium precursor approach yielded n-type electrical character. It is important for prospective electronic applications to identify analogous p-type systems. Solar cells, for example, rely on the formation of a junction between an n- and a p-type layer (with associated charge separation at the interface). The availability of both n-type and p-type transistors is also important for the realization of CMOS (complementary metal oxide semiconductor) technology for electronic circuit design.

Zinc telluride (ZnTe) is a relatively high mobility p-type semiconductor (~100 $cm^2\ V^{-1}\ s^{-1}$ for single-crystal material)

* E-mail: dmitzi@us.ibm.com.

(1) Mitzi, D. B.; Kosbar, L. L.; Murray, C. E.; Copel, M.; Afzali, A. *Nature* **2004**, *428*, 299.
(2) Mitzi, D. B. *J. Mater. Chem.* **2004**, *14*, 2355.
(3) Mitzi, D. B. *Inorg. Chem.* **2005**, *44*, 3755.
(4) Mitzi, D. B.; Copel, M.; Chey, S. J. *Adv. Mater.* **2005**, *17*, 1285.

10.1021/ic050833w CCC: $30.25
Published on Web 08/31/2005

with a direct band gap of ~2.25 eV,[5,6] which has been considered for use in light-emitting diode,[7] detector,[8] photovoltaic,[9−12] and transistor[13] applications. Copper-doped zinc telluride has been pursued, for example, as a potentially environmentally stable, low-resistance back-contact for CdS/CdTe solar cells.[11,12] Thin films of ZnTe are generally deposited using processes such as molecular beam epitaxy (MBE),[7,14] thermal evaporation,[11,13,15,16] electrodeposition,[10,17,18] and metal−organic vapor-phase epitaxy (MOVPE).[19,20] However, these approaches are not amenable to low-cost, large-area, high-throughput deposition. Some examples of techniques that fit these processing criteria include spin-coating, stamping, and printing, which, however, all require a soluble semiconductor or a soluble precursor that can be cleanly decomposed to the desired semiconductor at low temperature.

In this study, we report on the products formed using an ambient-temperature hydrazine solvent approach for dissolving ZnTe, analogous to that described for the main-group-metal sulfides and selenides.[1−4] Rather than forming ionic compounds containing discrete metal chalcogenide anions and hydrazinium cations (as observed for the main-group-metal sulfides and selenides under similar conditions), neutral hydrazine directly coordinates to the ZnTe framework and forms extended inorganic chains that interact with each other through van der Waals and hydrogen-bonding interactions. The resulting one-dimensional (1-D) ZnTe polymorphs α- and β-$(N_2H_4)_2ZnTe$ (**1** and **2**) are in contrast to a previously reported two-dimensional (2-D) structure, $(N_2H_4)ZnTe$, which was formed under solvothermal conditions employing a soluble zinc source and elemental tellurium.[21] Each of the two new precursors may be readily dissolved in hydrazine, solution processed onto substrates, and thermally decomposed to yield polycrystalline films of the p-type semiconductor ZnTe. While the zinc blende (cubic) form of ZnTe represents the most stable ZnTe polymorph,[15,22,23] bulk $(N_2H_4)_2ZnTe$ first decomposes to the wurtzite (hexagonal) form at temperatures as low as 200 °C, with a subsequent transformation to zinc blende ZnTe when annealed at temperatures above 350 °C. The hydrazine precursor approach therefore provides a convenient means of selectively forming cubic or hexagonal ZnTe.

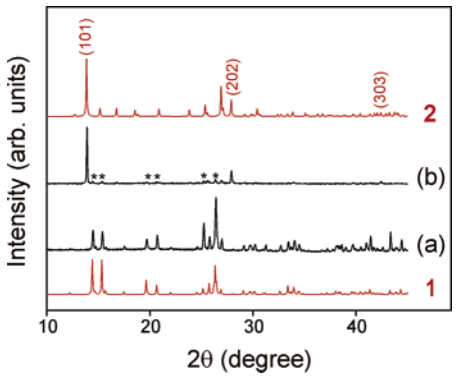

Figure 1. Powder X-ray diffraction patterns (Cu Kα radiation) for (a) bulk α-$(N_2H_4)_2ZnTe$ (**1**) and (b) a mixed-phase sample consisting of primarily β-$(N_2H_4)_2ZnTe$ (**2**), each prepared as described in the text. In (b) preferred orientation effects enhance the (*h*,0,*h*) reflections. The preferred orientation can be understood in terms of the orientation of the layers of chains within **2**, which are in the *a*−*c* plane (see the discussion of the structure in the text). The asterisks mark the positions of impurity peaks arising from **1**. The red curves (top and bottom) are simulations of the expected diffraction patterns for each polymorph, as determined using the single-crystal structure for each compound.

Experimental Section

Synthesis. α-$(N_2H_4)_2ZnTe$ (1). In an inert atmosphere at ambient temperature and pressure, 3 mmol of ZnTe (579.0 mg, Aldrich, 99.99%) and 3 mmol of Te (382.8 mg, Aldrich, 99.997%) are stirred with 40 mL of hydrazine (Aldrich, anhydrous, 98%) in a sealed flask. While ZnTe may, to a limited extent, dissolve in hydrazine, the addition of excess tellurium significantly improves the solubility and therefore the reaction yield. ***Caution:*** *Hydrazine is highly toxic and should be handled using appropriate protective equipment to prevent contact with either the vapors or the liquid.* The mixture is allowed to stir for 60 h, after which most of the reactants have gone into solution (a small amount of undissolved ZnTe remains in the flask). The solution is then filtered (still in an inert atmosphere) through a 0.2 μm syringe filter into a new flask, and 90 mL of 2-propanol (Aldrich, 99.5%, anhydrous) is gradually added with continuous stirring. The addition of 2-propanol leads to the formation of a lightly colored precipitate. The mixture is stirred for 1 h after the addition of the alcohol and then filtered through a medium frit. A mixture of methanol (Aldrich, 99.8%, anhydrous) and hydrazine (~3:2 ratio by volume), followed by pure methanol, is used to rinse excess tellurium from the product, yielding an off-white (very light brown) product. The product formed during this initial reaction is generally a mixture of **1** and **2** (with **1** being the dominant phase). The presence of **2** is most clearly indicated by the appearance of the (1,0,1) reflection from this phase in the powder X-ray pattern at $2\theta \approx 13.86°$ (see Figure 1b). Note that addition of substantially more 2-propanol to the solution during the precipitation step leads to excess tellurium in the product. A second dissolution and precipitation step in hydrazine

(5) Streetman, B. G. *Solid State Electronic Devices*; Prentice Hall: Englewood Cliffs, NJ, 1980; p 443.
(6) Tubota, H.; Suzuki, H.; Hirakawa, K. *J. Phys. Soc. Jpn.* **1961**, *16*, 1038.
(7) Sou, I. K.; Wong, K. S.; Yang, Z. Y.; Wang, H.; Wong, G. K. L. *Appl. Phys. Lett.* **1995**, *66*, 1915.
(8) Wu, Q.; Litz, M.; Zhang, X.-C. *Appl. Phys. Lett.* **1996**, *68*, 2924.
(9) Gashin, P.; Focsha, A.; Potlog, T.; Simashkevich, A. V.; Leondar, V. *Sol. Energy Mater. Sol. Cells* **1997**, *46*, 323.
(10) Aricò, A. S.; Silvestro, D.; Antonucci, P. L.; Giordano, N.; Antonucci, V. *Adv. Perform. Mater.* **1997**, *4*, 115.
(11) Feng, L.; Mao, D.; Tang, J.; Collins, R. T.; Trefny, J. U. *J. Electron. Mater.* **1996**, *25*, 1422.
(12) Gessert, T. A.; Mason, A. R.; Sheldon, P.; Swartzlander, A. B.; Niles, D.; Coutts, T. J. *J. Vac. Sci. Technol., A* **1996**, *14*, 806.
(13) Spînulescu-Carnaro, I. *Electron. Lett.* **1967**, *3*, 268.
(14) Yao, T.; Maekawa, S. *J. Cryst. Growth* **1981**, *53*, 423.
(15) Spînulescu-Carnaro, I. *Phys. Status Solidi* **1966**, *18*, 769.
(16) Ibrahim, A. A.; El-Sayed, N. Z.; Kaid, M. A.; Ashour, A. *Vacuum* **2004**, *75*, 189.
(17) (a) Ishizaki, T.; Ohtomo, T.; Fuwa, A. *J. Phys. D: Appl. Phys.* **2004**, *37*, 255. (b) Ishizaki, T.; Ohtomo, T.; Fuwa, A. *J. Electrochem. Soc.* **2004**, *151*, C161.
(18) Han, D.-H.; Choi, S.-J.; Park, S.-M. *J. Electrochem. Soc.* **2003**, *150*, C342.
(19) (a) Wolf, K.; Stanzl, H.; Naumov, A.; Wagner, H. P.; Kuhn, W.; Hahn, B.; Gebhardt, W. *J. Cryst. Growth* **1994**, *138*, 412. (b) Naumov, A.; Stanzl, H.; Wolf, K.; Rosenauer, A.; Lankes, S.; Gebhardt, W. *J. Cryst. Growth* **1994**, *138*, 595.
(20) Ogawa, H.; Irfan, G. S.; Nakayama, H.; Nishio, M.; Yoshida, A. *Jpn. J. Appl. Phys.* **1994**, *33*, L980.
(21) Huang, X.; Li, J.; Zhang, Y.; Mascarenhas, A. *J. Am. Chem. Soc.* **2003**, *125*, 7049.
(22) Däweritz, L. *Krist. Tech.* **1971**, *6*, 101.
(23) Yeh, C.-Y.; Lu, Z. W.; Froyen, S.; Zunger, A. *Phys. Rev. B* **1992**, *45*, 12130.

and 2-propanol, as described above, leads to approximately 440 mg of single-phase **1** (~57% yield based on the starting ZnTe). Indexing and refinement of the powder X-ray diffraction pattern (see Figure 1a) yields the lattice constants $a = 7.210(1)$ Å, $b = 11.549(1)$ Å, $c = 7.394(1)$ Å, and $\beta = 101.267(1)°$, with no impurity peaks detected. Chemical analysis (performed in duplicate by Galbraith Laboratories): observed, N (22.1), H (3.3); calculated for $(N_4H_8)ZnTe$, N (21.79), H (3.14). The product is readily soluble in hydrazine, but not substantially in other solvent systems examined (e.g., ethanolamine/DMSO mixtures, butylamine, DMF, 2-propanol).

A single crystal of **1** was grown by dissolving 50 mg of **1** in 3 mL of hydrazine, leading to a clear, essentially colorless solution (slight violet tinge). This solution was placed at the bottom of a long narrow tube (0.7 cm internal diameter, 30 cm long), with 3 mL of 2-propanol/hydrazine (mixed 50:50 by volume) and 9 mL of pure 2-propanol carefully layered on top (added to the tube with a long syringe needle). The layered crystal growth solution was allowed to sit undisturbed for 2 weeks, during which time a number of clear, colorless, well-formed crystals of **1** formed on the wall of the tube (near the central section), one of which was selected for single-crystal structure analysis.

***β*-$(N_2H_4)_2$ZnTe (2).** Isolation of single-phase **2** proved more difficult, suggesting that the formation of this polymorph may be thermodynamically less favorable. Crystals of **2** were isolated by dissolving 50 mg of **1**, prepared as described above, in 3 mL of hydrazine. Several drops of this solution were placed on a glass slide and allowed to evaporate in a glovebox over a period of approximately 1/2 h (under gently flowing nitrogen). The outer edge of the resulting deposit on the slide consisted of numerous clear, well-formed blocklike crystals, which proved to be primarily the polymorph **2**. One of these crystals was used to perform the single-crystal structure analysis described below. Some of the deposit was scraped off the slide and examined using powder X-ray diffraction, yielding the pattern in Figure 1b. While the deposit proved to be a mixture of **2** and **1**, **2** represented the majority phase. Chemical analysis (performed in duplicate by Galbraith Laboratories) of the deposit: observed, N (22.0), H (2.8); calculated for $(N_4H_8)ZnTe$, N (21.79), H (3.14). Note that slower crystallization from the above-described solution (e.g., by allowing the solution to evaporate in an open vial in the nitrogen-filled drybox over a period of several days) leads to the formation of a larger proportion of **1**.

Thin-Film Deposition. Zinc telluride (ZnTe) films were formed by drop-casting $(N_2H_4)_2$ZnTe solutions onto 19 mm diameter quartz disks, which were cleaned using a soap scrub/rinse, followed by sequential sonication in ethanol and dichloromethane and finally a "piranha" process (hydrogen peroxide/sulfuric acid in a 1:4 volume ratio, followed by a deionized water rinse). The solution for drop-casting was formed by dissolving 50 mg of α-$(N_2H_4)_2$ZnTe in 2.8 mL of hydrazine (Aldrich, anhydrous, 98%) to form a clear pale violet solution. The solution was found to be sensitive to air, turning darkly colored almost instantly upon exposure, and therefore, all processing involving the $(N_2H_4)_2$ZnTe/hydrazine solution was performed in a nitrogen-filled drybox with oxygen and water levels maintained below 1 ppm. When maintained in the drybox, the solution appeared to be stable for at least a week (longer times were not considered in this study). To form a drop-cast film, one drop of the solution (filtered through a 0.2 μm syringe filter) was placed onto a substrate. The solution spread to cover the substrate and was allowed to dry over a period of 1/2 h. Three drop-cast films were then heated for 1/2 h on a hot plate (in the drybox) at 250, 325, or 400 °C. The resulting films were nominally optically clear (transparent) and uniform, with the exception of a small amount of crystalline buildup around the edges of the substrate (this material was removed with a razor blade before further analysis). The resulting film thicknesses were in the range of 800−1000 Å, as measured using a Tencor Instruments Alpha Step 200 profilometer (at a step, produced using a razor blade, near the center of each film).

Table 1. Crystallographic Data for $(N_2H_4)_2$ZnTe (**1** and **2**)

	α-$(N_2H_4)_2$ZnTe (**1**)	*β*-$(N_2H_4)_2$ZnTe (**2**)
chemical formula		
fw	257.08	257.08
space group	*P*21 (No. 4)	*Pn* (No. 7)
a, Å	7.2157(4)	8.1301(5)
b, Å	11.5439(6)	6.9580(5)
c, Å	7.3909(4)	10.7380(7)
β, deg	101.296(1)	91.703(1)
V, Å^3	603.72(6)	607.17(7)
Z	4	4
ρ_{calcd}, g/cm^3	2.828	2.812
wavelength, Å	0.71073 (Mo Kα)	0.71073 (Mo Kα)
abs coeff (μ), cm^{-1}	86.8	86.4
R^a	1.53	1.49
$R_w{}^b$	1.92	1.85

$^a R = \sum(|F_o| - |F_c|)/\sum(|F_o|)$. $^b R_w = \{\sum w(|F_o| - |F_c|)^2/\sum(w|F_o|^2)\}^{1/2}$.

Powder X-ray Diffraction (XRD). XRD powder patterns were collected for the two $(N_2H_4)_2$ZnTe polymorphs, the bulk thermal decomposition products of **1** formed at various temperatures, and the solution-deposited ZnTe films, using a Siemens D5000 diffractometer (Cu Kα radiation). The specimens for bulk analysis were prepared by pressing powder of the sample into vacuum grease on a glass slide. Thin-film samples were prepared by drop-casting on quartz disks as described above. The amorphous background from the quartz disk was measured separately and subtracted. The phases present in each sample were identified (e.g., ZnTe, Te) by comparison with powder diffraction file (PDF) cards or, in the case of the new compounds **1** and **2**, by comparison with the calculated powder patterns from the single-crystal structures (see Figure 1). In these latter cases, the powder patterns were generated using the Mercury (v.1.3) program (CCDC).[24] Where refinement of lattice constants was performed from the diffraction data (i.e., Figure 1a, bulk α-$(N_2H_4)_2$ZnTe (**1**), and Figure 8, TGA decomposition products of **1**), initial cell constants from the PDF card (for ZnTe) or from the single-crystal structure (for **1**) were used. Pawley refinement[25] was used to optimize the diffraction pattern parameters using the Accelrys MS Modeling package. The peak profiles were fitted using a pseudo-Voigt function. The final Pawley refinement R_{wp} values were 6.7% for the α-$(N_2H_4)_2$ZnTe (**1**) data in Figure 1a, 10.0% for the cubic ZnTe data (425 °C) in Figure 8, 11.0% for the hexagonal ZnTe data (350 °C) in Figure 8, 6.1% for the hexagonal ZnTe data (300 °C) in Figure 8, and 4.8% for the hexagonal ZnTe data (200 °C) in Figure 8.

X-ray Crystallography. A clear (essentially colorless) α-$(N_2H_4)_2$ZnTe (**1**) [*β*-$(N_2H_4)_2$ZnTe (**2**)] platelike [irregular blocklike] crystal, with the approximate dimensions 0.03 mm × 0.15 mm × 0.30 mm [0.06 mm × 0.06 mm × 0.11 mm], was selected under a microscope and attached to the end of a quartz fiber with 5 min epoxy. Intensity data were collected with a Bruker SMART CCD diffractometer equipped with a fine focus 2.4 kW sealed tube X-ray source (Mo Kα radiation), with a detector distance of approximately 5.0 cm, in 2272 frames with increasing ω, and an exposure time of 30 s [40 s] per frame. The increment in ω between each frame was 0.3°.

Final unit cell parameters (Table 1) and the crystal orientation matrix were obtained by a least-squares fit of 6011 [4730]

(24) Bruno, I. J.; Cole, J. C.; Edgington, P. R.; Kessler, M.; Macrae, C. F.; McCabe, P.; Pearson, J.; Taylor, R. *Acta Crystallogr.* **2002**, *B58*, 389.
(25) Pawley, G. S. *J. Appl. Crystallogr.* **1981**, *14*, 357.

Table 2. Selected Bond Distances (Å) and Angles (deg) for α-$(N_2H_4)_2ZnTe$ (**1**)

Zn1−Te1	2.6197(6)	Zn1−Te1−Zn2	105.68(2)
Zn1−Te2	2.5839(7)	Zn1−Te2−Zn2[a]	99.53(2)
Zn1−N1	2.097(4)	Te1−Zn1−Te2	122.53(3)
Zn1−N3	2.115(5)	Te1−Zn1−N1	111.4(1)
Zn2−Te1	2.5798(6)	Te1−Zn1−N3	105.2(1)
Zn2−Te2[b]	2.5836(6)	Te2−Zn1−N1	105.1(1)
Zn2−N5	2.089(5)	Te2−Zn1−N3	115.1(1)
Zn2−N7	2.103(4)	N1−Zn1−N3	93.8(2)
N1−N2	1.443(7)	Te1−Zn2−Te2[b]	127.58(2)
N3−N4	1.465(6)	Te1−Zn2−N5	111.0(1)
N5−N6	1.462(7)	Te1−Zn2−N7	106.7(1)
N7−N8	1.437(6)	Te2[b]−Zn2−N5	105.6(1)
		Te2[b]−Zn2−N7	103.1(1)
		N5−Zn2−N7	99.0(2)
		Zn1−N1−N2	113.5(3)
		Zn1−N3−N4	118.2(3)
		Zn2−N5−N6	111.8(3)
		Zn2−N7−N8	115.4(3)

[a] $1 + x, y, z$. [b] $-1 + x, y, z$.

reflections. An empirical absorption correction based on equivalent reflections was applied to the intensity data.[26] The structure was solved and refined using the NRCVAX 386 PC version program.[27] First, the Zn and Te atoms were located using direct methods. The N atoms were then located using successive Fourier difference maps. For **2**, one nitrogen atom (N4) exhibited large and anisotropic thermal parameters when refined using a fully ordered model. The thermal parameters were improved, however, when this nitrogen was disordered over two sites, and therefore, the disordered-nitrogen model was ultimately chosen for final refinement. Hydrogen atoms were located from difference maps and fully refined using isotropic thermal parameters. The minimum and maximum peaks in the final difference Fourier maps corresponded to −0.50 and +0.51 e/Å^3 [−0.40 and +0.38 e/Å^3]. For **1**, the Flack parameter for the chiral structure was refined to 0.13(4). No additional symmetry was detected for the refined structures using the MISSYM program.[28] Attempts to refine the heavy atom (Zn, Te, N) site occupancies led to no evidence for vacancies on any of these sites for either **1** or **2**. Therefore, while the possibility of trace levels of vacancies or stoichiometry variations cannot entirely be ruled out, **1** and **2** appear to have the same composition to within the resolution of the structure refinement and chemical analysis measurements performed. Crystallographic results for the two compounds are summarized in Table 1. Selected bond lengths for each of the compounds are given in Tables 2 and 3. A complete listing of crystallographic data (in CIF format) is given as Supporting Information.

Thermal Analysis. Thermogravimetric analysis **(**TGA) scans were performed, using a TA Instruments TGA-2950 system, in a flowing nitrogen atmosphere and with a 5 °C/min ramp to 425 °C. The thermal analysis apparatus was also used to decompose samples of **1** at selected temperatures below 425 °C. Each thermal treatment was based on a 5 °C/min ramp to the desired temperature, *T*, followed by a dwell at the final temperature for an amount of time equal to (425 − *T*)/5 min. In this way, each sample experienced the same length of overall heat treatment as the sample heated to 425 °C (for which there was no dwell). After thermal decomposition, each sample was examined by X-ray diffraction for phase analysis.

Table 3. Selected Bond Distances (Å) and Angles (deg) for β-$(N_2H_4)_2ZnTe$ (**2**)

Zn1−Te1	2.5914(7)	Zn1−Te1−Zn2	100.30(2)
Zn1−Te2[b]	2.5902(9)	Zn1[a]−Te2−Zn2	104.86(2)
Zn1−N1	2.107(6)	Te1−Zn1−Te2[b]	114.41(2)
Zn1−N7	2.083(6)	Te1−Zn1−N1	113.7(2)
Zn2−Te1	2.5905(7)	Te1−Zn1−N7	108.0(2)
Zn2−Te2	2.5752(7)	Te2[b]−Zn1−N1	110.5(2)
Zn2−N3	2.115(6)	Te2[b]−Zn1−N7	112.8(2)
Zn2−N5	2.089(5)	N1−Zn1−N7	96.0(2)
N1−N2	1.443(8)	Te1−Zn2−Te2	118.87(3)
N3−N4a	1.47(1)	Te1−Zn2−N3	110.2(2)
N3−N4b	1.46(3)	Te1−Zn2−N5	105.7(2)
N5−N6	1.449(9)	Te2−Zn2−N3	111.4(2)
N7−N8	1.432(8)	Te2−Zn2−N5	112.3(2)
		N3−Zn2−N5	95.8(2)
		Zn1−N1−N2	117.3(5)
		Zn1−N7−N8	113.6(4)
		Zn2−N3−N4a	115.8(6)
		Zn2−N3−N4b	106(1)
		Zn2−N5−N6	110.6(4)

[a] $0.5 + x, 1 - y, -0.5 + z$. [b] $-0.5 + x, 1 - y, 0.5 + z$.

Differential scanning calorimetry (DSC) thermograms were also collected on a TA Instruments MDSC-2920 under a nitrogen purge and using a 5 °C/min temperature ramp rate. The aluminum sample pans for the DSC measurement were sealed with a top lid. However, a small hole was punched into the lid to allow the decomposition products (evolved gases) to escape from the container.

Results and Discussion

Synthetic and Phase Relation Issues. Recently, the layered monohydrazine compound $(N_2H_4)ZnTe$ was isolated by reacting $Zn(NO_3)_2{\cdot}6H_2O$, tellurium, and hydrazine under solvothermal conditions (110 °C).[21] The compound crystallizes in the chiral monoclinic space group $P2_1$, and zinc and tellurium atoms are alternatively three-coordinated to each other, leading to puckered 6^3 2-D ZnTe slabs. The nitrogen from a hydrazine molecule completes the tetrahedral coordination for each zinc atom, with the hydrazine molecules extending out into the space between the slabs. The 2-D compound $(N_2H_4)ZnTe$ represents an example of a more general family of covalently bonded amine-based metal chalcogenide frameworks [e.g., $(en)_{1/2}ZnTe$, $(pda)_{1/2}ZnTe$, (pda)ZnTe, (ma)ZnTe, $(en)_{1/2}Cd_{1-x}Mn_xSe$, $(pda)_{1/2}CdSe$ (en = ethylenediamine, pda = propanediamine, ma = methylamine)], all formed under solvothermal conditions.[21,29−32] In each case, the compounds are formed at elevated temperature through a reaction among a non-chalcogenide metal salt (e.g., a nitrate, acetate, carbonate, sulfate, or chloride), a chalcogen source, and an appropriate amine-based solvent/reactant.

This structural family is particularly interesting because each member represents a lower dimensional slice from the three-dimensional (3-D) metal chalcogenide framework, with associated quantum confinement effects noted in the electronic properties. By changing the organic linker and dimensionality of the inorganic network, single-sized and periodically ordered arrays of nanostructures (e.g., metal

(26) Sheldrick, G. M. *SADABS*; Institut für Anorganische Chemie der Universität Göttingen: Göttingen, Germany, 1997.
(27) Gabe, E. J.; Le Page, Y.; Charland, J.-P.; Lee, F. L.; White, P. S. *J. Appl. Crystallogr.* **1989**, *22*, 384.
(28) Le Page, Y. *J. Appl. Crystallogr.* **1988**, *21*, 983.
(29) Huang, X.; Li, J. *J. Am. Chem. Soc.* **2000**, *122*, 8789.
(30) Huang, X.; Li, J. *Mater. Res. Soc. Symp. Proc.* **2002**, *728*, S1.7.1.
(31) Lu, J.; Wei, S.; Yu, W.; Zhang, H.; Qian, Y. *Chem. Mater.* **2005**, *17*, 1698.
(32) Deng, Z.-X.; Li, L.; Li, Y. *Inorg. Chem.* **2003**, *42*, 2331.

chalcogenide chains, sheets) have been demonstrated.[21] In addition, the layered amine-based chalcogenide systems have been identified as potential intermediates in the formation of metal chalcogenide nanorods.[32,33] While the structural and electronic properties of these systems have been reported, ambient-temperature solubility and film formation have not been extensively discussed.

The reactions reported in this Article are remarkable because they comprise directly dissolving the metal chalcogenide semiconductor (rather than a nitrate, acetate, carbonate, sulfate, or chloride salt) in the solvent (hydrazine + tellurium), reducing the likelihood of contaminants in the final product from the counteranion of the salt or its decomposition product (e.g., Cl^-, CH_3COO^-). Additionally, dissolution occurs at ambient temperature, rather than under elevated-temperature conditions, providing a simpler ("softer") synthetic route. The resulting two polymorphs **1** and **2** appear to be fairly close in terms of their relative stability, as initial precipitation of $(N_2H_4)_2ZnTe$ from a hydrazine/Te solution using 2-propanol generally yields a mixture of the two phases (**1**, however, is the majority phase). If a hydrazine solution of $(N_2H_4)_2ZnTe$ (containing no extra Te) is allowed to slowly evaporate (over several days), in an open vial under inert-atmosphere conditions, **1** appears as the dominant polymorph formed. When the same solution is more rapidly evaporated by placing drops of the solution on a glass slide and having them evaporate over a period of 1/2 to 1 h, **2** appears to become more prevalent (no single-phase bulk samples of **2** have been prepared to date, however). Therefore, **1** may be the more thermodynamically favored phase, with the formation of **2** being kinetically driven. It is interesting, however, that, during precipitation from hydrazine solutions using 2-propanol (a relatively quick process), **1** appears as the majority phase. Therefore, the reaction medium also appears to play a role in which phase is ultimately stabilized. Additional studies are warranted to further differentiate the conditions favoring the formation of **1** versus **2**, as well as to elucidate the energetics and stabilities of the two polymorphs.

Interestingly, Li et al.[33] have previously reacted Zn and Te in hydrazine hydrate under solvothermal conditions (at ~170 °C) and achieved a precursor for nanorod formation, which they proposed to have a $(N_2H_4)_2ZnTe$ stoichiometry. However, no chemical analysis or structural characterization was provided to support this assignment. Furthermore, the reported powder X-ray diffraction pattern for the product does not match that of either **1** or **2**, and the color of the product (black) is not consistent with the quantum confinement effects provided by a 1-D system (**1** and **2** are essentially colorless crystals). Finally, in contrast with the results in the current study (wherein hexagonal ZnTe is achieved upon low-temperature thermal decomposition; see discussion below), cubic ZnTe was achieved upon low-temperature thermal decomposition (at 250 °C) in the previous study.[33] It is therefore doubtful that the product of this earlier study was either **1** or **2**. Indeed, given the low

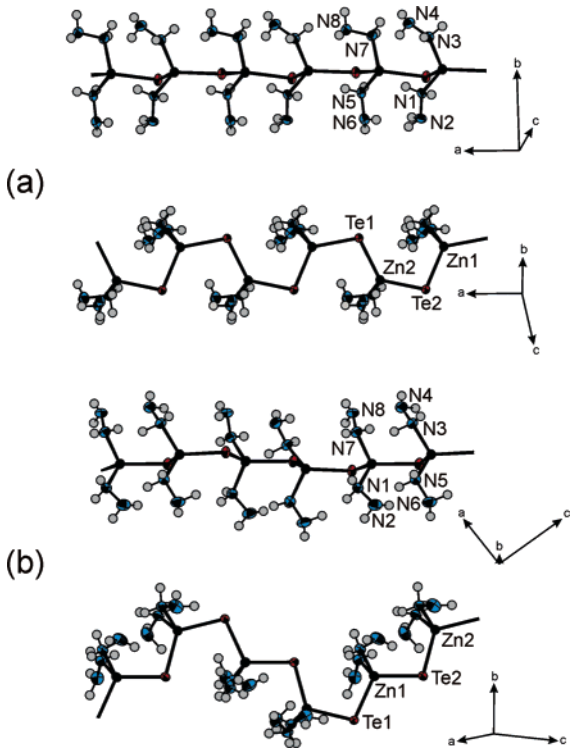

Figure 2. Detailed structure (two views) of the $(N_2H_4)_2ZnTe$ chains in (a) α-$(N_2H_4)_2ZnTe$ (**1**) and (b) β-$(N_2H_4)_2ZnTe$ (**2**), with atom labeling shown. The thermal ellipsoids for Zn, Te, and N atoms are drawn at 50% probability. For clarity, hydrogen atoms are represented as spheres, with an arbitrarily selected uniform size, and only one of the two disordered N4 nitrogens is shown (for **2**).

decomposition temperature (~85 °C) observed for $(N_2H_4)_2ZnTe$ (see discussion below), it is not surprising that **1** and **2** would not be formed either under the solvothermal conditions employed by Li et al.[33] or during the synthesis of $(N_2H_4)ZnTe$ reported by Huang et al.,[21] since these reactions were carried out at elevated temperatures. Interestingly, among the compounds previously reported, (pda)ZnTe (the only other reported 1-D member of this family of lower dimensional chalcogenides) was formed at the relatively low temperature of 70 °C in a mixture of hydrazine and pda.[21] Higher temperature reactions (above 120 °C) in pure pda led to the formation of $(pda)_{0.5}ZnTe$, which is comprised of 2-D ZnTe sheets. In this respect, it appears that lower temperatures are helpful in stabilizing the 1-D structures.

Crystal Structures. The crystal structures of both **1** and **2** consist of 1-D $(N_2H_4)_2ZnTe$ chains (Figure 2), with van der Waals and hydrogen-bonding interactions among the chains. In chiral α-$(N_2H_4)_2ZnTe$ (**1**), the chains extend down the *a* axis (i.e., [1,0,0]) of the structure (Figure 3), while in β-$(N_2H_4)_2ZnTe$ (**2**) the chains are oriented along [1,0,−1] (Figure 4). For each structure, the Zn atoms are tetrahedrally coordinated to two Te atoms and two N atoms (from monodentate hydrazine molecules). The Zn−Te bond lengths range from 2.5798(6) to 2.6197(6) Å (2.5918 Å average) for **1** and from 2.5752(7) to 2.5914(7) Å (2.5868 Å average) for **2**, while the Te−Zn−Te bond angles are 122.53(3)°/127.58(2)° for **1** and 114.41(5)°/118.87(3)° for **2** (Tables 2 and 3). These Te−Zn−Te bond angles, which are slightly larger than the ideal 109.5° tetrahedral angle, are counter-

(33) Li, Y.; Ding, Y.; Wang, Z. *Adv. Mater.* **1999**, *11*, 847.

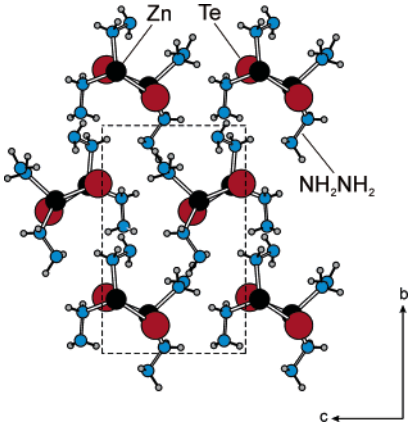

Figure 3. Crystal structure of α-$(N_2H_4)_2ZnTe$ (**1**), viewed down [1,0,0] (the direction of chain propagation). Dashed lines indicate the unit cell outline. For clarity, atoms are represented as spheres, with uniform sizes selected for each atom type.

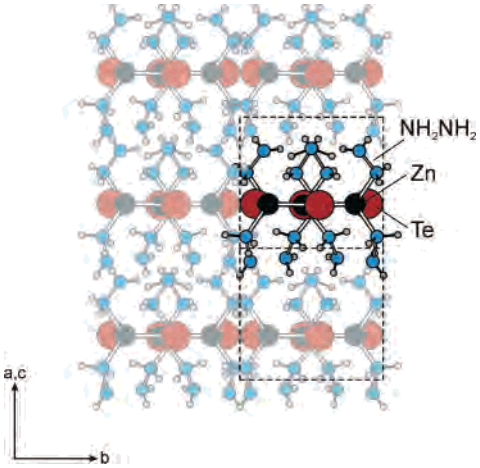

Figure 4. Crystal structure of β-$(N_2H_4)_2ZnTe$ (**2**), viewed down [1,0,−1] (the direction of chain propagation). Dashed lines indicate the unit cell outline. For clarity, atoms are represented as spheres, with uniform sizes selected for each atom type, and only one of the two disordered N4 nitrogens is shown. The highlighted (darker line) component of the structure shows the boundary of a single chain.

balanced by slightly compressed N−Zn−N bond angles—93.8(2)°/99.0(2)° for **1** and 95.8(2)°/96.0(2)° for **2**. Each Te atom is bonded to two Zn atoms, thereby completing the formation of 1-D ZnTe chains, with Zn−Te−Zn bond angles of 99.53(2)°/105.68(2)° for **1** and 100.30(2)°/104.86(2)° for **2**.

Despite the relatively similar local Zn and Te coordination in each compound, the chains in **1** and **2** adopt distinct conformations (Figure 2). The two conformations can be considered alternative slices from the 2-D $(N_2H_4)ZnTe$ structure, as shown in Figures 5 and 6. Of the previously studied amine-based covalently bonded metal chalcogenide structures, only the (pda)ZnTe structure exhibits 1-D ZnTe chains analogous to those found in the title compounds, with the other reported systems exhibiting higher dimensional metal chalcogenide networks.[21] Indeed, the conformation of the (pda)ZnTe chains is similar to that reported in **1**, while the conformation found in **2** has apparently not been previously reported.

Interaction between $(N_2H_4)_2ZnTe$ chains in **1** and **2** is through van der Waals and/or hydrogen-bonding interactions

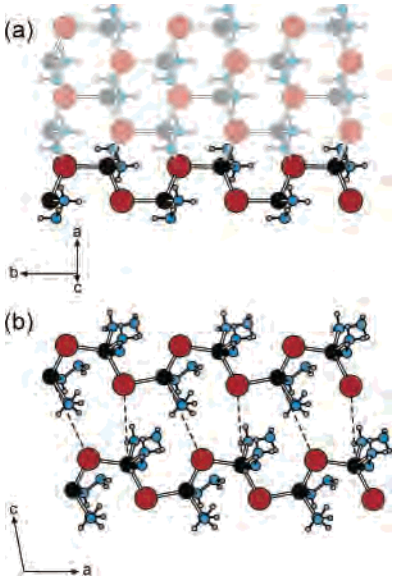

Figure 5. (a) A single layer from the previously reported $(N_2H_4)ZnTe$ structure,[21] as viewed perpendicular to the layer. For clarity, atoms are represented as spheres, with uniform sizes selected for each atom type (atom labeling as in Figure 3). The highlighted section of the sheet shows how the $(N_2H_4)_2ZnTe$ chain from α-$(N_2H_4)_2ZnTe$ (**1**) can be conceptually cut from the layered structure. (b) Two adjacent $(N_2H_4)_2ZnTe$ chains from **1** in the *a*−*c* crystallographic plane. The dashed lines indicate a possible route to condense these chains into layers of $(N_2H_4)ZnTe$ (with the loss of a hydrazine molecule at each Zn atom).

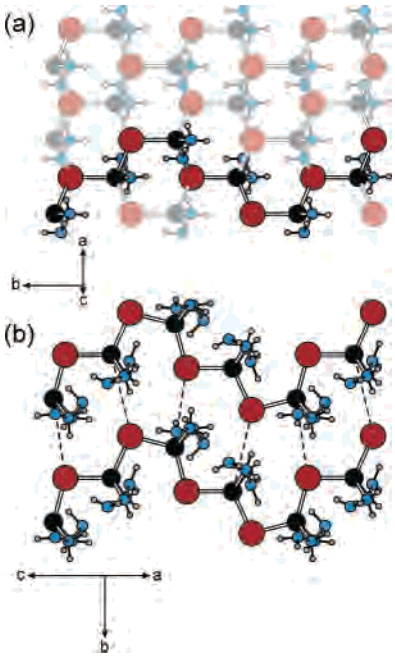

Figure 6. (a) A single layer from the previously reported $(N_2H_4)ZnTe$ structure,[21] as viewed perpendicular to the layer. For clarity, atoms are represented as spheres, with uniform sizes selected for each atom type (atom labeling as in Figure 3). The highlighted section of the sheet shows how the $(N_2H_4)_2ZnTe$ chain from β-$(N_2H_4)_2ZnTe$ (**2**) can be conceptually cut from the layered structure. (b) Two adjacent $(N_2H_4)_2ZnTe$ chains from **2** in a [1,0,1] plane. The dashed lines indicate a possible route to condense these chains into layers of $(N_2H_4)ZnTe$ (with the loss of a hydrazine molecule at each Zn atom).

among pendent hydrazine molecules on adjacent chains. Multiple short N···N contact distances among nitrogens on adjacent chains range from 3.007(6) to 3.061(5) Å for **1**, substantially shorter than the shortest interlayer N···N

contacts in $(N_2H_4)ZnTe$ (3.738 Å). The N−H···N bond angles for these interactions range from ∼151° to 172°. The short N···N contacts are both among $(N_2H_4)_2ZnTe$ chains in the same layer of chains ($a-c$ plane), as well as among chains on adjacent layers (Figure 3). For **2**, a single short (<3.15 Å) N···N contact, 3.058(8) Å, links chains stacked parallel to [1,0,1] (Figure 4). The interchain N···N interactions among the layers of chains defined by [0,1,0] and [1,0,−1] (as in Figure 6b) are substantially weaker, perhaps because of the more undulating nature of the chains in **2**, as well as because of the manner in which the pendent hydrazines alternate sides on the ZnTe chains in **2** (i.e., alternating two on one side and two on the other; compare parts a and b of Figure 2). The less intimate N···N contacts in **2**, relative to **1**, may suggest a less efficient packing of the chains, as is also reflected in the slightly lower calculated density for **2** (2.812 versus 2.828 g/cm^3), despite the same stoichiometry. This may partially account for the fact that **2** appears to be more difficult to stabilize in single-phase bulk form (i.e., it appears to be thermodynamically less stable, as discussed above).

Thermal Analysis. An important feature of the previously reported hydrazinium-based precursors,[1−4] with respect to their use in the solution deposition of metal chalogenide semiconductors, is the low temperature at which the precursors decompose. For the metal chalcogenide hydrazinium salts $(N_2H_4)_x(N_2H_5)_yM^{+n}{}_zX_{(zn+y)/2}$, where M is a metal (e.g., Ge, Sn, In, Sb) with valence n and X is a chalcogen (e.g., S, Se, Te), decomposition generally occurs by loss of the x molecules of hydrazine, followed by loss of the protonated hydrazinium moiety and correspondingly $y/2$ chalcogens.[1,3] This latter transition can occur either as a loss of hydrazine and hydrogen chalcogenide (e.g., as H_2S or H_2Se) or as loss of decomposition products of these species (e.g., as H_2 and S or Se). Note that hydrogen chalcogenides can readily decompose to hydrogen and chalcogen at moderate temperatures[34] and metal chalcogenides may act to catalyze this reaction.[35] While, in the case of the sulfides, the precursors generally decompose at low temperature (∼200 °C),[1] for the corresponding selenides, excess selenium (presumably from the decomposition of H_2Se) does not evolve from the sample until ∼350 °C or, in some cases, even higher temperatures.[3] This is likely because of both the reduced stability of H_2Se relative to the corresponding sulfide (note that H_2Te is even less stable—essentially thermodynamically unstable with respect to the constituent elements)[36] and the lower volatility of Se versus S.[3] For prospective hydrazinium salts based on metal tellurides, the decomposition process is likely to be shifted further to higher temperatures (in excess of 450 °C), because of the lower volatility of Te, well outside the range of interest for thin-film deposition on flexible plastic substrates (Kapton, one of the highest temperature plastics, can withstand temperatures as high as 400 °C).

The fact that the product formed from dissolution of ZnTe in hydrazine (followed by evaporation of the solvent) is a covalent compound, rather than a salt, is therefore beneficial with respect to minimizing the temperature of the decomposition process. For the formation of ZnTe from $(N_2H_4)_2$-ZnTe, only hydrazine (no tellurium-containing species) needs to evolve from the sample. Because of the relatively weak coordination of hydrazine, the decomposition reaction is expected to be a low-temperature process. Additionally, the small molecular size of hydrazine implies that the weight and volume loss during decomposition should be minimized. For $(N_2H_5)_4Sn_2S_6$, the expected weight loss during thermal decomposition to SnS_2 is ∼34.9% (resulting from the loss of both hydrazine and hydrogen sulfide), while, for $(N_2H_4)_2$-ZnTe, the weight loss in the formation of ZnTe is only 24.9%. The smaller materials loss from deposited precursor films should facilitate more uniform final film morphology after annealing (e.g., avoiding possible cracks and voids).

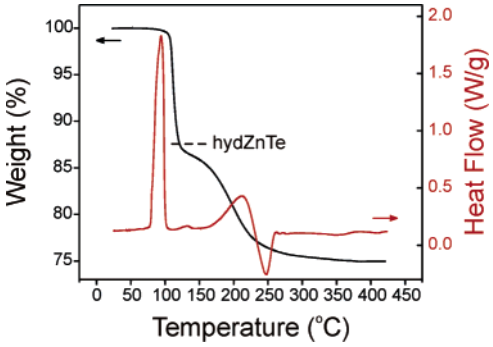

Figure 7. TGA and DSC of **1** (5 °C/min ramp rate, nitrogen atmosphere). The dashed line indicates the weight loss value corresponding to the composition $(N_2H_4)ZnTe$.

Figure 7 shows the thermal decomposition and differential scanning calorimetry profiles for α-$(N_2H_4)_2ZnTe$ (**1**). Decomposition of the precursor to ZnTe occurs in approximately two steps and is completed by ∼200−250 °C. The overall observed weight loss (24.9% at 350 °C) is in good agreement with that expected for the formation of ZnTe from **1**. The first thermal transition, beginning as early as 80 °C and yielding a weight loss of ∼13.3% at 130 °C, corresponds approximately with what would be expected for the loss of one hydrazine molecule from $(N_2H_4)_2ZnTe$ (12.5%), with the resulting formation of the 2-D compound $(N_2H_4)ZnTe$.[21] X-ray diffraction studies of this intermediate decomposition product (Figure 8) support the assignment of this phase to $(N_2H_4)ZnTe$ (or a closely related phase), as does chemical analysis performed on the product: expected, N (12.45), H (1.79); found, N (12.1), H (1.7). Note that there is a very natural condensation reaction (with the loss of one hydrazine molecule for each Zn atom) that may occur within the layers of chains for both the α and β phases of $(N_2H_4)_2ZnTe$, which would be expected to yield the 2-D $(N_2H_4)ZnTe$ sheets with minimal molecular rearrangement (Figures 5 and 6). It is likely, however, that this process would not be perfect and that there would also be limited condensation occurring between adjacent $(N_2H_4)ZnTe$ sheets (i.e., cross-linking) in the intermediate decomposition product. This may partially account for the significant peak broadening and unusual preferred orientation effects [i.e., not corresponding to the

(34) Pearson, R. K.; Haugen, G. R. *Int. J. Hydrogen Energy* **1981**, *6*, 509.
(35) Chivers, T.; Lau, C. *Int. J. Hydrogen Energy* **1987**, *12*, 235.
(36) Cotton, F. A.; Wilkinson, G. *Advanced Inorganic Chemistry*, 4th ed.; John Wiley & Sons: New York, 1980; p 511.

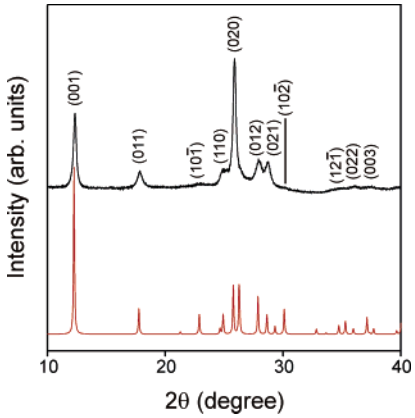

Figure 8. Powder X-ray diffraction pattern (Cu Kα radiation) for the decomposition product formed by heating α-$(N_2H_4)_2ZnTe$ (**1**) to 95 °C and terminating the isotherm after ~12.5% weight loss (~35 min). The red curve is a simulation of the expected diffraction pattern for $(N_2H_4)ZnTe$, as determined using the single-crystal structure.[21] The reflection indices noted in the figure are also based on this $(N_2H_4)ZnTe$ single-crystal structure.

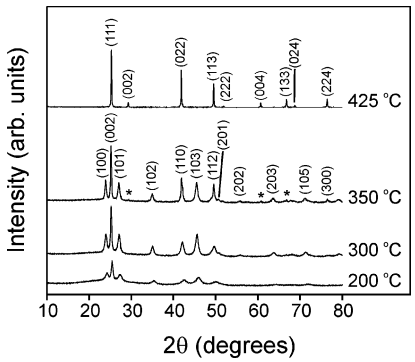

Figure 9. Powder X-ray diffraction patterns (Cu Kα radiation) for **1** after heating to various temperatures between 200 and 425 °C (using the same conditions as those for the TGA scans), demonstrating formation of bulk ZnTe. Indexing of the diffraction pattern for the 350 °C data is given based on the wurtzite (hexagonal) form of ZnTe (PDF 19-1482), while that for the 425 °C data is given based on zinc blende (cubic) ZnTe (PDF 15-0746). The asterisks (350 °C data) mark the positions of cubic ZnTe "impurity" reflections starting to appear in the diffraction pattern for the otherwise wurtzite ZnTe sample.

most natural cleavage plane of $(N_2H_4)ZnTe$] in the X-ray data of Figure 8. Interestingly, the most pronounced (relative to the expected pattern) and sharpest peaks in the diffraction pattern of Figure 8 are the reflections along [0,1,0], which is along a direction parallel to the original chains of **1** (see Figure 5). Reflections involving components along the *a* axis (i.e., the direction in which the chains condense) are systematically the weakest and broadest.

To further evaluate the decomposition process of the title 1-D compounds **1** and **2** into the 3-D ZnTe semiconductor, the X-ray diffraction profiles of decomposition products formed by heating **1** to various temperatures (Figure 9) have been examined. Decomposition to crystalline ZnTe can be seen to occur at temperatures as low as 200 °C. Interestingly, the phase formed at these lower temperatures is wurtzite ZnTe, rather than the more thermodynamically stable zinc blende form.[15,22,23] The refined hexagonal cell volume appears to increase slightly with higher processing temperatures, and the refined crystallite size increases substantially as well (as indicated by the degree of peak broadening). The refined

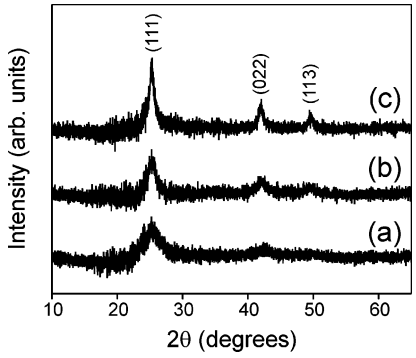

Figure 10. Powder X-ray diffraction patterns (Cu Kα radiation) for thin films of ZnTe deposited (as described in the text) from solutions of **1**, with final thermal treatment at (a) 250 °C, (b) 325 °C, or (c) 400 °C. Indexing of the diffraction pattern for (c) is given based on the zinc blende (cubic) form of ZnTe (PDF 15-0746).

lattice constants for the hexagonal structures are as follows: a = 4.278(2) Å, c = 7.051(3) Å (200 °C data); a = 4.303(1) Å, c = 7.088(2) Å (300 °C data); a = 4.322(1) Å, c = 7.108(1) Å (350 °C data). Deng et al.[32] have suggested that the preferential decomposition of $(en)_{1/2}ZnX$ and $(en)_{1/2}CdX$ (X = S, Se, Te) into the wurzite polymorph of the respective metal chalcogenide may be attributed to structural similarities between the 2-D precursor and the wurtzite polymorph of the metal chalcogenide. Since the 1-D polymorphs **1** and **2** apparently transform into the 2-D system $(N_2H_4)ZnTe$ as they condense into ZnTe, a similar templating mechanism may be operative in the thermal decomposition of the title compounds into wurtzite ZnTe. At temperatures above 350 °C, however, the initial hexagonal wurtzite diffraction pattern transforms to that of the cubic zinc blende polymorph (Figure 9). The refined lattice constant (a = 6.106(1) Å) for the cubic ZnTe product formed at 425 °C is in good agreement with literature values.[37]

Film Deposition. The ability to put ZnTe into a hydrazine-based solution, as well as the low decomposition temperatures of the resulting 1-D precursors, enables the convenient deposition of ZnTe films on a diverse range of substrates. In principle, the solutions could be spin-coated, ink-jet-printed, spray-coated, doctor-bladed, painted, or dip-coated. In the current study, drop-casting is used to demonstrate thin-film deposition. The films are formed by placing a drop of the $(N_2H_4)_2ZnTe$ hydrazine solution onto a quartz substrate and allowing it to spread and dry, yielding a film of ZnTe after thermal decomposition. Figure 10 shows the X-ray diffraction patterns for similarly prepared films, with the only difference being the final annealing temperature (varied from 250 to 400 °C). For each choice of annealing temperature, the film appears to be crystalline, with improving crystallinity for the higher temperature anneals. Note that increasing the film annealing time (at a given temperature) from 1/2 to 6 h only very slightly influences the resulting diffraction pattern (i.e., sharper more intense peaks). The films also all appear to adopt the zinc blende ZnTe polymorph for all temperatures although, given the weak nature of the diffraction pattern, it is difficult to unambiguously distinguish between the two

(37) Swanson, H. E.; Morris, M. C.; Evans, E. H.; Ulmer, L. *NBS Monogr.* **1964**, *No. 25* (Sect. 3), 58.

phases. While vacuum-based evaporation studies have also overwhelmingly yielded films with the cubic structure,[11,15,16,38] Spînulescu-Carnaru[15] have established that the Zn:Te ratio in the evaporation plume can influence the polymorph formed in the resulting vapor-phase-deposited films, with a more zinc rich mixture favoring the formation of the hexagonal phase. Other factors influencing the choice of ZnTe polymorph in the evaporated films included film thickness, deposition temperature, and background pressure in the deposition chamber.[15]

Conclusion

The hydrazinium precursor approach for metal chalcogenide film deposition has proven quite useful among metal sulfide and selenide systems. The technique relies on the formation of a highly soluble hydrazinium-based salt of the metal chalcogenide, which can decompose at relatively low temperature to the targeted metal chalcogenide semiconductor (or metal or insulator) after solution deposition into thin-film form. Inherent in the decomposition step is the need to evolve extra chalcogen from the sample (from the chalcogenide anion) to form the phase-pure metal chalcogenide film. As a result of the decreasing stability of the H_2X moiety[36] and decreasing volatility of the chalcogens (X = S, Se, Te) with increasing atomic number, unacceptably high temperatures would likely be required to yield a phase-pure sample of metal telluride using the hydrazinium salt technique (if indeed such a precursor could even be stabilized).

This study has demonstrated that, like many main-group-metal sulfides and selenides, ZnTe readily dissolves in hydrazine/Te solutions under ambient-temperature conditions. However, the resulting product formed upon evaporation of the hydrazine solvent is not a salt, but rather the covalent 1-D polymorphs α- and β-$(N_2H_4)_2$ZnTe. As these compounds are readily soluble in hydrazine and only lose hydrazine during thermal decomposition to ZnTe, the process of ZnTe thin-film deposition or bulk semiconductor formation using solutions of these precursors can be completed at low temperature (as low as 200 °C). While the chemistry of ZnTe dissolution in hydrazine (i.e., formation of covalently bonded hydrazine zinc telluride chains) appears to be quite different from that for the analogous main-group-metal sulfides and selenides (formation of hydrazinium salts), the room-temperature dissolution of each of these systems in hydrazine-based solvents, generally with excess chalcogen, highlights the remarkable (though not universal) solvent capabilities of hydrazine with respect to the family of metal chalcogenides.

Metal chalcogenides offer a range of interesting electronic characteristics, ranging from insulators to semiconductors (n- and p-type) and metals. The ability to dissolve the metal chalcogenides in hydrazine or hydrazine-like solvents thereby opens the possibility to solution-deposit a range of different thin-film device components, including those for solar cell, transistor, memory, and thermoelectric applications. In addition to the potential practical implications of a convenient thin-film deposition process, the current polymorphs α- and β-$(N_2H_4)_2$ZnTe represent two of the few examples of 1-D covalently bonded amine-based metal chalcogenide systems [with the other structurally characterized example being (pda)ZnTe].[21] The systems **1** and **2** are therefore important new members of this family of lower dimensional structures and are expected to demonstrate quantum confinement effects similar to those observed from the other family members. Interestingly, the polymorphs **1** and **2** are found to decompose first to the lower stability wurtzite ZnTe polymorph, before transforming to the zinc blende variant at higher temperatures. Since either polymorph of ZnTe can ultimately be formed by appropriate choice of the annealing temperature, the hydrazine precursor route provides a selective pathway to the formation of bulk wurtzite or zinc blende ZnTe.

Finally, we have demonstrated solution-processed thin films of the semiconductor ZnTe, prepared using the drop-casting technique and hydrazine-based solutions of α-$(N_2H_4)_2$-ZnTe. Preliminary experiments using these drop-cast (or analogously spin-coated) films as semiconducting TFT channel layers yielded p-type behavior, although only low mobilities (<0.001 cm^2 V^{-1} s^{-1}).[39] A number of factors could negatively impact the measured field-effect mobility in these unoptimized devices, including small grain size/insufficient grain connectivity, limited current injection (i.e., inappropriate choice of metal contacts), the channel layer being too thick/thin, or impurities (undistilled hydrazine was used and all reagents were used "as received" in the current experiment). Each of these factors will need to be examined to fully evaluate the potential for use of these films in TFTs as well as in other devices. It will also be of interest to explore whether p-type (e.g., Cu)[11,12,38] and n-type (e.g., Al)[20] dopants can be incorporated into the solution-processed ZnTe films and whether the present low-temperature film deposition technique employing soluble covalently bonded amine-based metal chalcogenide precursors can be extended beyond the ZnTe system.

Supporting Information Available: An X-ray crystallographic file, in CIF format, containing information for $(N_2H_4)_2$ZnTe (**1** and **2**). This material is available free of charge via the Internet at http://pubs.acs.org.

IC050833W

(38) Goyal, D. J.; Bilurkar, P. G.; Thorat, S. K.; Mate, N. V. *Mater. Res. Soc. Symp. Proc.* **1998**, *485*, 261.

(39) Mitzi, D. B. Unpublished results.